

2. S.E. Sussman-Fort and R.M. Rudish, Non-foster impedance matching of electrically-small antennas, *IEEE Trans Antennas Propag* 57 (2009).
3. J.R. Jahoda, JTRS/SINCGARS ultrabroadband airborne blade antenna for subsonic aircraft and helicopters, *Defence Electron* (2006) 20–22.
4. S.R. Best, A discussion on electrically small antennas loaded with high permittivity and permeability materials, In: *International Workshop on Antenna Technology (iWAT)*, IEEE, 7–9 March 2011, pp. 90–93.
5. I. Tzanidis, C.-C. Chen, and J.L. Volakis, Smaller UWB conformal antennas for VHF/UHF applications with ferroelectric loadings, In: *Antennas and Propagation Society International Symposium*, IEEE, San Diego, CA, 2008, pp. 1–4.
6. B.A. Kramer, M. Lee, C.-C. Chen, and J.L. Volakis, A miniature conformal spiral antenna using inductive and dielectric loading, In: *Antennas and Propagation Society International Symposium*, IEEE, Honolulu, HI, 2007, pp. 1004–1007.
7. J.L. Volakis, C.C. Chen, and K. Fujimoto, *Small antennas: miniaturization techniques and application*, 2010.
8. S.M.A. Momeni Hasan Abadi and N. Behdad, An electrically small, vertically polarized ultrawideband antenna with monopole-like radiation characteristics, *IEEE Antennas Wireless Propag Lett* 13 (2014).
9. N. Behdad, M. Li, and Y. Yusuf, A very low-profile, omnidirectional, ultrawideband antenna, *IEEE Antennas Wireless Propag Lett* 12 (2013).
10. J. Zhao, C.C. Chen, and J.L. Volakis, Frequency-scaled UWB inverted-hat antenna, *IEEE Trans Antennas Propag* 58 (2010), 2447–2451.
11. I.A. Osaretin, A. Torres, and C.C. Chen, A novel compact dual-linear polarized UWB antenna for VHF/UHF applications, *IEEE Antennas Wireless Propag Lett* 8 (2009), 145–148.
12. H. Moon, G.Y. Lee, C.C. Chen, and J.L. Volakis, An extremely low-profile ferrite-loaded wideband VHF antenna design, *IEEE Antennas Wireless Propag Lett* 11 (2012), 322–325.
13. K.L. Lau, P. Li, and K.M. Luk, A monopolar patch antenna with very wide impedance bandwidth, *IEEE Trans Antennas Propag* 53 (2005), 655–661.
14. W.J. Lu, Y.F. Weng, S.W. Cheung, and H.B. Zhu, Compact top-loaded ultra-wideband biconical antenna for indoor base-station applications, *Microwave Opt Technol Lett* 52 (2010), 2594–2598.
15. J.M. Gonzalez-Arbescu and E. Romeu, On the influence of fractal dimension on radiation efficiency and quality factor of self-resonant pre-fractal wire monopoles, In: *Antennas and Propagation Society International Symposium*, IEEE, Vol. 4, Honolulu, HI, 2003, pp. 214–217.
16. K. Noguchi, M. Mizusawa, T. Yamaguchi, and Y. Okumura, Increasing the bandwidth of a meander line antenna consisting of two strips, In: *Antennas and Propagation Society International Symposium*, IEEE, Montreal, Quebec, 1997, pp. 2198–2201.

© 2015 Wiley Periodicals, Inc.

3.6-GHz 10-ANTENNA ARRAY FOR MIMO OPERATION IN THE SMARTPHONE

Kin-Lu Wong and Jun-Yu Lu

Department of Electrical Engineering, National Sun Yat-sen University, Kaohsiung 80424, Taiwan; Corresponding author: wongkl@ema.ee.nsysu.edu.tw

Received 17 December 2014

ABSTRACT: A 10-antenna array operating in the 3.6-GHz band (3400–3800 MHz) for multi-input multi-output (MIMO) operation in the smartphone is presented. Each antenna in the proposed array is a microstripline-fed open-slot antenna with same small dimensions of $3 \times 8 \text{ mm}^2$ ($0.036\lambda \times 0.096\lambda$, λ is the wavelength at 3.6 GHz). The proposed

array consists of two symmetric five-antenna arrays disposed, respectively, along two long side edges of the system ground plane of the smartphone. The proposed array is expected to be placed in the narrow spacing between the display panel and the long side edges of the smartphone. Acceptable isolation (better than about 10 dB) and good envelop correlation coefficient (ECC) of less than 0.1 for any two antennas in the proposed array is obtained. The maximum channel capacity of the proposed array in a 10×10 MIMO system is calculated to reach about 47 bps/Hz at 20-dB signal-to-noise ratio, which is larger than four times that (11.5 bps/Hz) of the upper limit of an ideal 2×2 MIMO system with 100% antenna efficiency and zero ECC between antennas. Details of the proposed 10-antenna array are described, and the experimental results are presented and discussed. © 2015 Wiley Periodicals, Inc. *Microwave Opt Technol Lett* 57:1699–1704, 2015; View this article online at wileyonlinelibrary.com. DOI 10.1002/mop.29181

Key words: mobile antennas; multi-input multi-output antennas; 10-antenna array; smartphone antennas; small antennas

1. INTRODUCTION

For mobile communications, it is known that multi-input multi-output (MIMO) operation can lead to a much higher channel capacity for enhanced data throughput [1, 2]. When more antennas are included in the MIMO operation, much higher channel capacity can be obtained. However, owing to the very limited space in the smartphone for accommodating the internal antennas, it is a great design challenge on embedding more antennas within the smartphone. Recently, the four-antenna array [3, 4] or eight-antenna array [5] for the LTE MIMO operation in the smartphone have been reported. The four-antenna array in [3] can be applied for the 4×4 MIMO operation in the 1880–2690 MHz band. In [4], the four-antenna array consists of one two-antenna array at the top edge and one two-antenna array at the bottom edge [6] and can cover the 750–960 and 1710–2690 MHz bands for the 4×4 MIMO operation. The eight-antenna array reported in [5] is for the LTE 3.5-GHz (3400–3600 MHz) band operation. It is shown that the ergodic channel capacity for a 2×8 MIMO system at 20-dB signal-to-noise ratio (SNR) can reach about 15.5 bps/Hz [5], which is better than (about 11.5 bps/Hz [1]) of an ideal 2×2 MIMO system with 100% antenna efficiency and zero envelop correlation coefficient (ECC) between antennas.

In this article, we present a 10-antenna array operating in the 3.6-GHz band (3400–3800 MHz) for the MIMO operation in the smartphone. The proposed array consists of two five-antenna arrays disposed, respectively, along two long side edges of the system ground plane of the smartphone. The antennas in the proposed array are microstripline-fed open-slot antennas and can be easily fabricated in the system ground plane. Each antenna has same dimensions and can fit in the narrow spacing between the display panel and the long side edges of the smartphone. The proposed array is also fabricated and tested. Any two antennas in the proposed array show acceptable isolation of better than about 10 dB and good ECC of less than 0.1 in the 3.6-GHz band.

From the measured three-dimensional complex radiation patterns and antenna efficiencies of each antenna in the fabricated array, the maximum ergodic channel capacity of the 10-antenna array in a 10×10 MIMO system is calculated to reach about 47 bps/Hz at 20-dB SNR. The obtained channel capacity is larger than four times that (about 11.5 bps/Hz [1]) of an ideal MIMO system (100% antenna efficiency and zero ECC between antennas).

In this study, details of the proposed array and the antenna geometry therein are described. Simulated and experimental

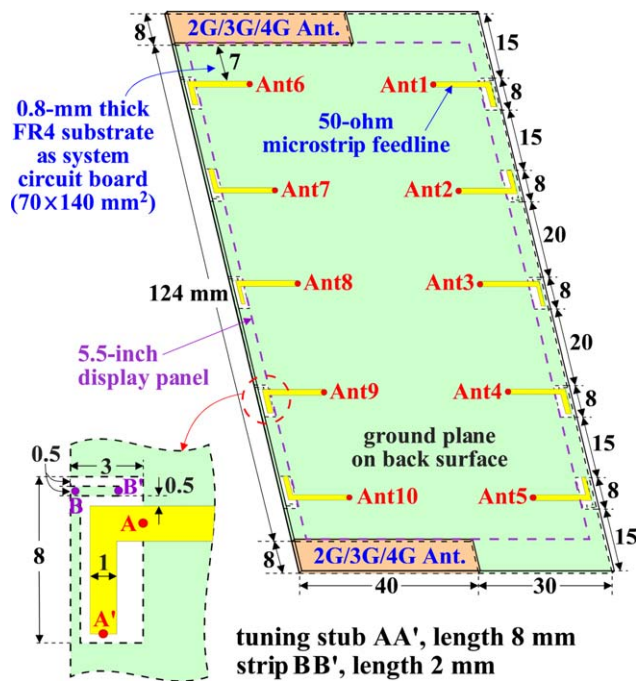


Figure 1 Geometry of the 3.6-GHz 10-antenna array for the MIMO operation in the smartphone. [Color figure can be viewed in the online issue, which is available at wileyonlinelibrary.com]

results of the impedance and radiation performance of each antenna in the proposed array are presented. The ECC between antennas and the ergodic channel capacity of the proposed array in a 10×10 MIMO system are also calculated and discussed.

2. PROPOSED 10-ANTENNA ARRAY

2.1. Array Structure and Antenna Geometry Therein

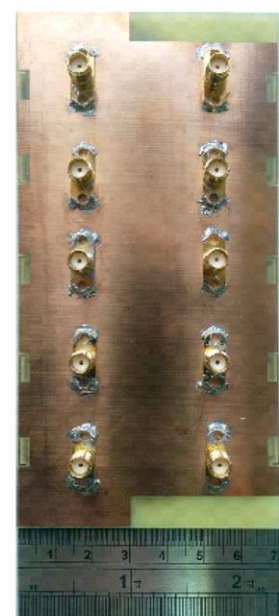
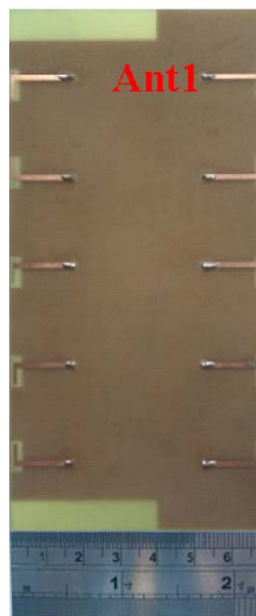
The proposed 10-antenna array for the MIMO operation in the smartphone is shown in Figure 1. The proposed array is also fabricated and tested. The photos of the fabricated 10-antenna array in this study are shown in Figure 2. The proposed array is disposed in a system ground plane of $140 \times 70 \text{ mm}^2$ for a typical 5.5-inch smartphone. The proposed array is formed by two same five-antenna arrays printed along two long side edges of the system ground plane. Note that the system ground plane in this study is printed on a 0.8-mm thick FR4 substrate of relative permittivity 4.4 and loss tangent 0.02. The two rectangular clearance regions of $8 \times 40 \text{ mm}^2$ at the top and bottom edges of the system ground plane are reserved for accommodating two LTE/WWAN antennas for the 2G/3G/4G operation, such as the antenna reported in [7] that can cover the 698–960 and 1710–2690 MHz bands with a compact antenna size to fit in the reserved clearance regions. The two antennas to be disposed in the two clearance regions, however, are not included in this study.

Each antenna in the proposed array is a microstripline-fed open-slot antenna [8–10] with same dimensions of $3 \times 8 \text{ mm}^2$ ($0.036\lambda \times 0.096\lambda$, λ is the wavelength at 3.6 GHz). The 50- Ω microstrip feedline has an inverted-L tuning stub (section AA') of length 8 mm inside the open slot. At the opening of the open slot, there is a short strip (section BB') of length 2 mm added to provide an enhanced capacitance at the open slot, which can make the excited open-slot resonant mode shifted to lower frequencies. The required open-slot dimensions for covering the 3.6-GHz band can hence be decreased. In this study, the length

of the open slot is 8 mm, which is only about 0.1λ at 3.6 GHz. Also, note that the tuning stub of section AA' is extended away from the opening. This arrangement can lead to good excitation of the open-slot resonant mode. Each five-antenna array disposed at the right or left long edge of the system ground plane is formed by two antenna pairs and an antenna at the center thereof. The two antenna pairs at the right long edge are (Ant1, Ant2) and (Ant4, Ant5), while those at the left long edge are (Ant6, Ant7) and (Ant9, Ant10). Ant3 and Ant8 are disposed at the center of the right and left long edges, respectively. The two antennas in each antenna pair have a spacing of 15 mm (about 0.18λ at 3.6 GHz) and are arranged to have their openings at the outer-most boundary of the antenna pair, which can lead to acceptable isolation (better than about 10 dB) between two antennas in the antenna pair. This is mainly because strong electric fields generally occur at the opening of the open slot, hence

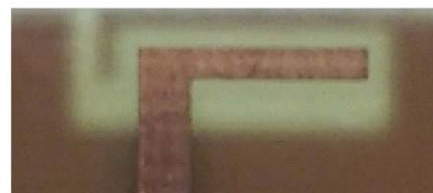
front view

back view



(a)

Ant1 front view

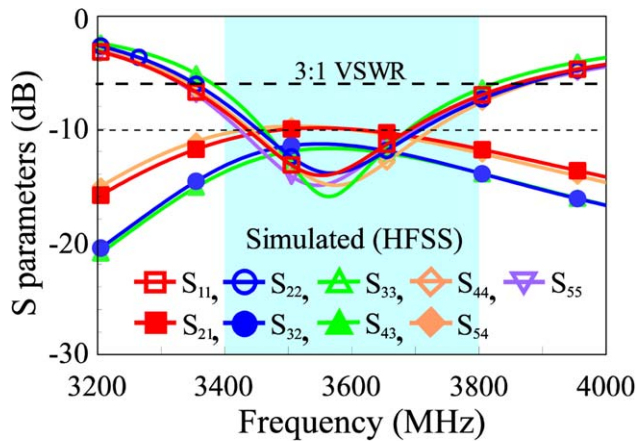


Ant1 back view

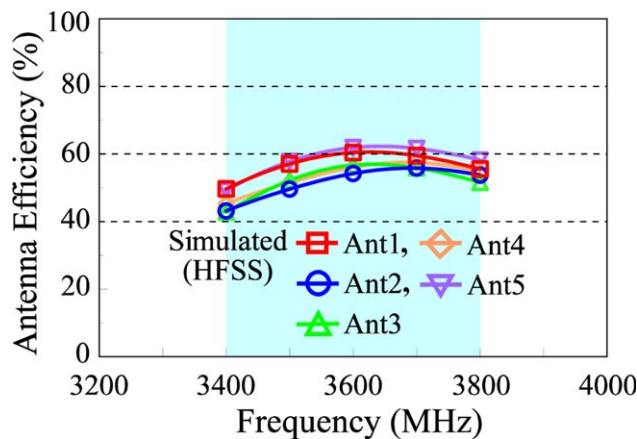


(b)

Figure 2 (a) Photos of the fabricated 10-antenna array. (b) Enlarged photo of Ant1 in the 10-antenna array. [Color figure can be viewed in the online issue, which is available at wileyonlinelibrary.com]



(a)



(b)

Figure 3 Simulated (a) S parameters and (b) antenna efficiency for Ant1 to Ant5. [Color figure can be viewed in the online issue, which is available at wileyonlinelibrary.com]

larger spacing between the two openings can lead to decreased coupling between two antennas. Also, note that each antenna pair has a length of 31 mm only (about 0.37λ at 3.6 GHz), and the antennas therein can have wide bandwidths to cover the 3.6-GHz band (3.4–3.8 GHz).

For Ant3 and Ant8, they are disposed between two antenna pairs and have a distance of 20 mm (about 0.24λ at 3.6 GHz) to the two antenna pairs. As the distance is at least about a quarter-wavelength, acceptable isolation of Ant3 and Ant8 to other antennas in the proposed array can be obtained. Ant3 and Ant8 can also have wide bandwidths to cover the desired 3.6-GHz band.

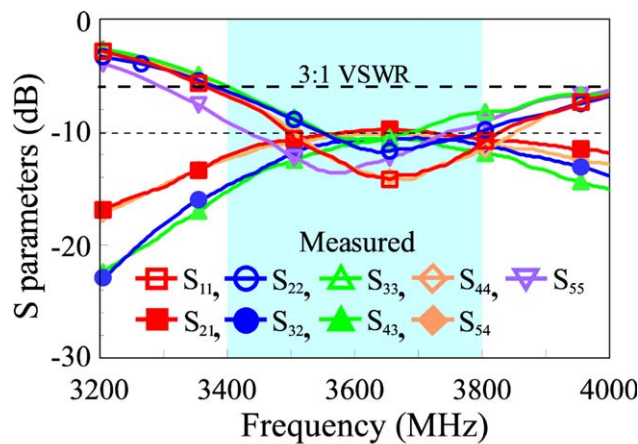
2.2. Antenna Performance

The antenna performance of Ant1 to Ant10 in the proposed 10-antenna array is first studied. Figure 3(a) shows the simulated S parameters for Ant1 to Ant5, and the antenna efficiency which includes mismatching losses is shown in Figure 3(b). The simulated results are obtained using the full-wave electromagnetic field simulator HFSS version 15 [11]. The impedance matching of Ant1 to Ant5 is all better than 6 dB (3:1 VSWR) for frequencies in the 3.6-GHz band (see the shaded frequency region in the figure). The isolation between the antenna pair of (Ant1, Ant2) and (Ant4, Ant5) is also seen to be better than about 10 dB. The isolation of Ant3 to Ant2 and Ant4 is even better than about 12 dB.

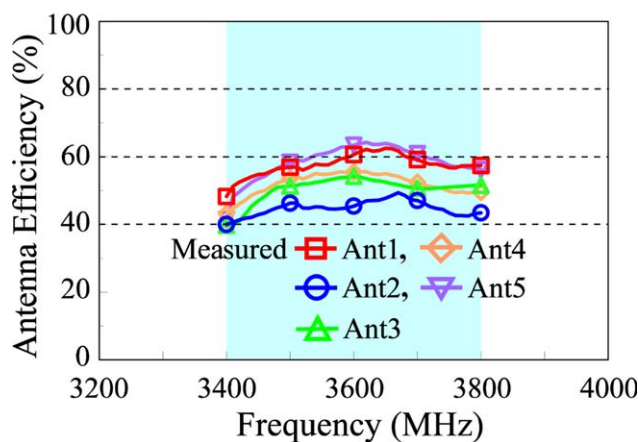
From the results shown in Figure 3(b), acceptable antenna efficiency for Ant1 to Ant5 is also obtained. The antenna efficiency of Ant1 and Ant5 is about 50–62%, while that of Ant2, Ant3, and Ant4 is about 42–56%. The results indicate that Ant1 and Ant5 which are disposed at the outer-most boundary of the antenna array can have better antenna efficiency. Conversely, the antenna efficiency of Ant2, Ant3, and Ant4 which have nearby antennas at their two sides is slightly lower.

The fabricated 10-antenna array shown in Figure 2 was also tested. The measured S parameters and antenna efficiency for Ant1 to Ant5 are presented in Figure 4. It is seen that the measured data in Figure 4 generally agree with the simulated results in Figure 3.

The antenna performance for Ant6 to Ant10 at the left long edge of the system ground plane is also shown for comparison. The simulated results of the S parameters and antenna efficiency for Ant6 to Ant10 are shown in Figure 5, while the corresponding measured data are presented in Figure 6. Agreement between the simulation and measurement is also obtained. Owing to the two clearance regions at the left long edge of the system ground plane, Ant6 and Ant10 have a short distance of 7 mm (about 0.08λ at 3.6 GHz) to the ground edge. This short distance leads to a degradation in the impedance matching of Ant6 and Ant10, as compared with that of Ant1 and Ant5 which have a distance of 15 mm (about 0.18λ at 3.6 GHz) to the ground edge [see the curves of S_{66} and S_{1010} in Fig. 5(a) vs.



(a)



(b)

Figure 4 Measured (a) S parameters and (b) antenna efficiency for Ant1 to Ant5. [Color figure can be viewed in the online issue, which is available at wileyonlinelibrary.com]

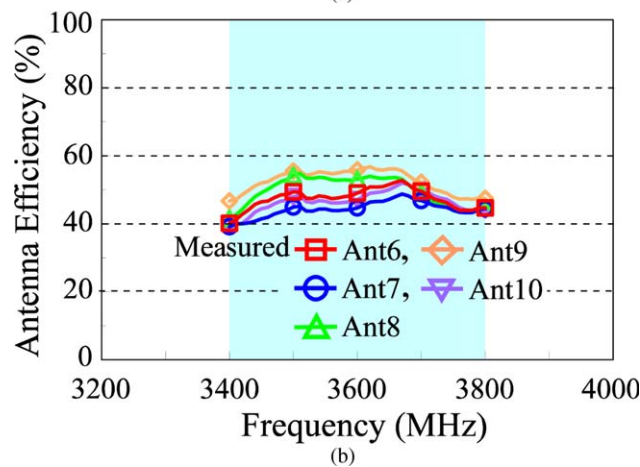
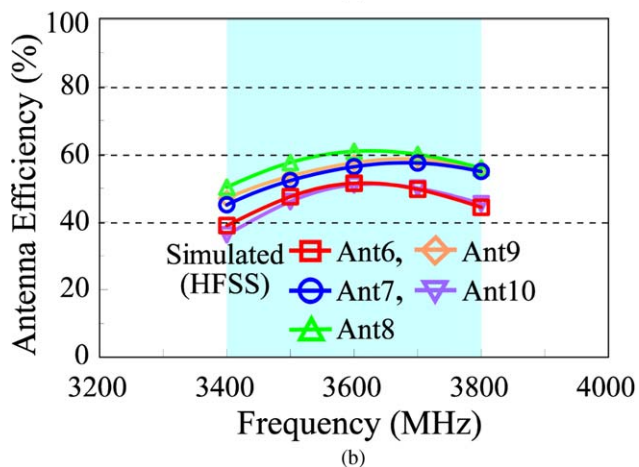
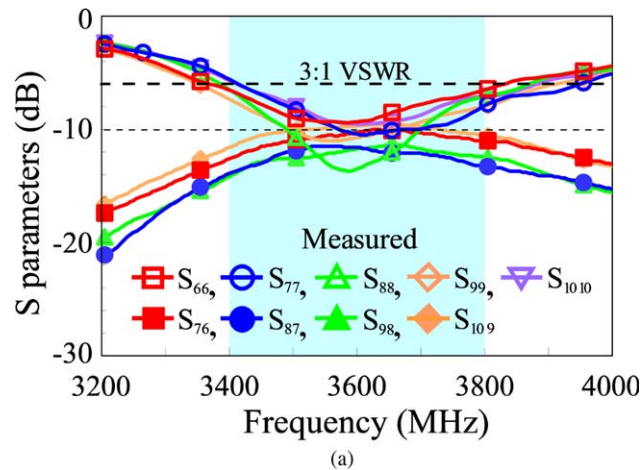
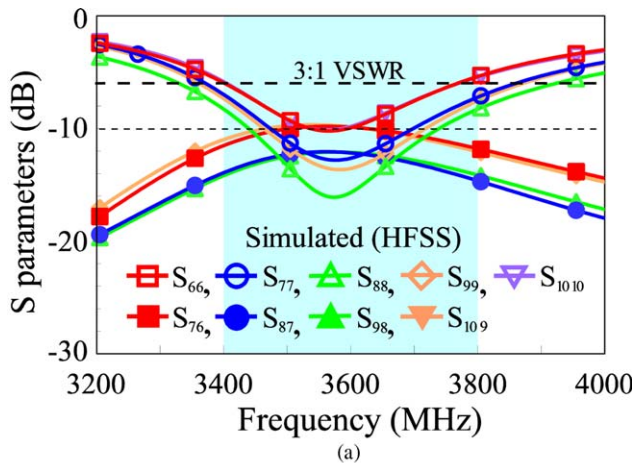


Figure 5 Simulated (a) S parameters and (b) antenna efficiency for Ant6 to Ant10. [Color figure can be viewed in the online issue, which is available at wileyonlinelibrary.com]

Figure 6 Measured (a) S parameters and (b) antenna efficiency for Ant6 to Ant10. [Color figure can be viewed in the online issue, which is available at wileyonlinelibrary.com]

those of S_{11} and S_{55} in Fig. 3(a)]. From the measured S parameters shown in Figure 6(a), however, the impedance matching of Ant6 to Ant10 is all less than about -6 dB in the 3.6-GHz band. The isolation between any two antennas in the antenna array of Ant6 to Ant10 is also all better than about 10 dB. The obtained results are similar to the observations for the antenna array of Ant1 to Ant5.

It is also observed that the degradation in the impedance matching makes the antenna efficiency of Ant6 and Ant10 lower than that of Ant7, Ant8, and Ant9. From the results shown in Figure 5(b), the antenna efficiency of Ant6 and Ant10 is about 38–51%, and that of Ant7, Ant8, and Ant9 is about 45–62%. The measured data shown in Figure 6(b) indicates that the antenna efficiency of Ant6 to Ant10 is all better than about 40% and varies in the range of 40–57%. The measured antenna efficiency generally agrees with the simulated results.

To analyze the excited open-slot resonant mode of the antennas in the proposed array, the simulated electric field and surface current distributions at 3.6 GHz for Ant1 and Ant3 as representatives of all the antennas are shown in Figure 7. Strong electric fields are seen to occur at the opening of the open slot and gradually decrease to the closed end of the open slot. Strong surface currents along the outer edge, closed edge, and inner edge of the open slot are also excited. The observed behavior indicates that the open slot resonant mode is excited [8–10].

The measured and simulated three-dimensional radiation patterns for the antennas in the proposed array are presented in Figures 8 and 9. Figure 8 shows the results for Ant1 to Ant5, and those for Ant6 to Ant10 are shown in Figure 9. Agreement between the simulated and measured radiation patterns is generally obtained. It is also seen that each antenna has a unique radiation pattern, different from those of other antennas. This behavior is advantageous for achieving smaller ECCs between antennas in the proposed 10-antenna array, thereby an enhanced

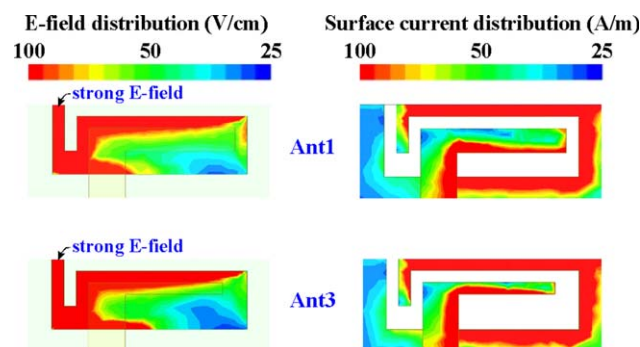


Figure 7 Simulated electric field and surface current distributions at 3.6 GHz for Ant1 and Ant3. [Color figure can be viewed in the online issue, which is available at wileyonlinelibrary.com]

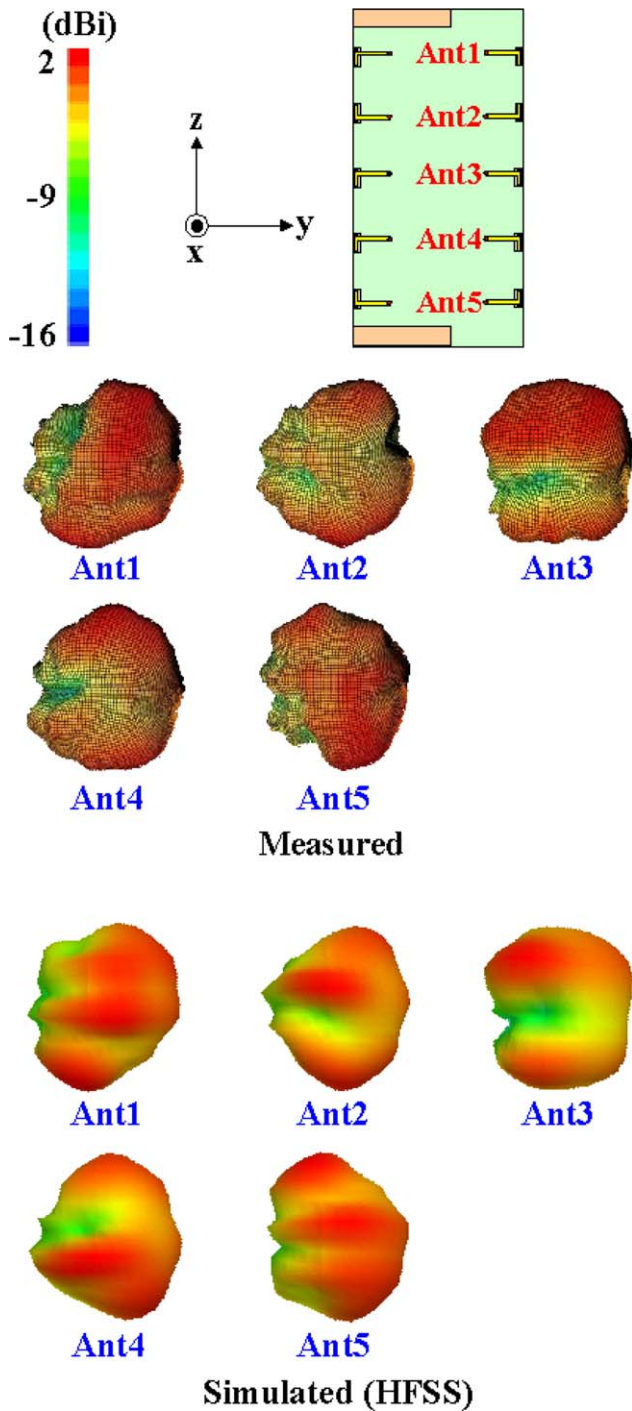


Figure 8 Measured and simulated three-dimensional radiation patterns for Ant1 to Ant5. [Color figure can be viewed in the online issue, which is available at wileyonlinelibrary.com]

channel capacity for the 10×10 MIMO operation can be obtained.

3. MIMO PERFORMANCE

To analyze the MIMO performance of the proposed 10-antenna array in a 10×10 MIMO system, the calculated ECC from the measured complex electric-field patterns and simulated ECC from the HFSS [11] is presented in Figure 10. Typical ECC

results between Ant1 and Ant2, Ant1 and Ant3, Ant2 and Ant3, Ant2 and Ant4, and Ant1 and Ant6 are presented. The ECC results are obtained by assuming the indoor propagation environment with a uniform incident wave [12]. Good agreement between the ECC results shown in Figures 10(a) and 10(b) is seen. The ECC values are all less than 0.1 in the 3.6-GHz band, which is good for the MIMO operation.

Figure 11 shows the calculated ergodic channel capacities of the fabricated 10-antenna array in a 10×10 MIMO system. The uncorrelated transmitting antennas and the independently identically distributed (i.i.d.) channels with Rayleigh fading

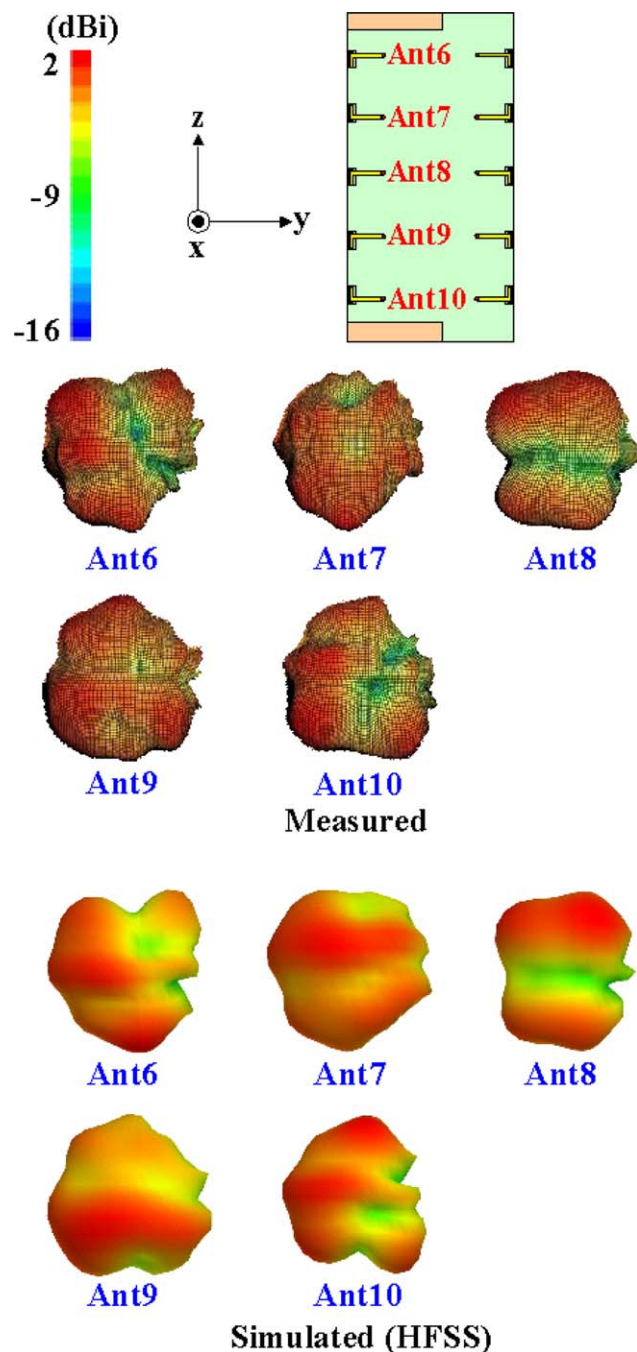


Figure 9 Measured and simulated three-dimensional radiation patterns for Ant6 to Ant10. [Color figure can be viewed in the online issue, which is available at wileyonlinelibrary.com]

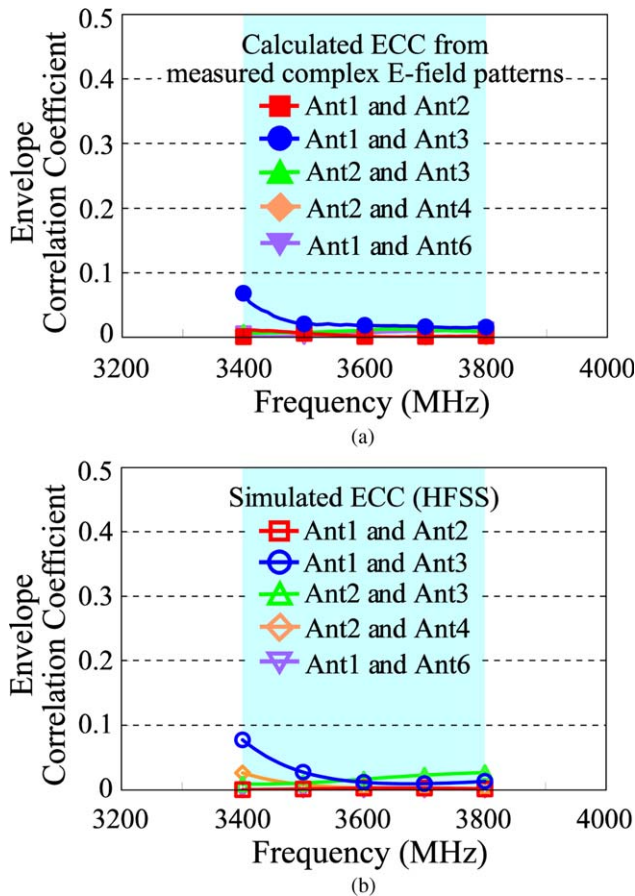


Figure 10 (a) Calculated ECC from the measured complex electric-field patterns and (b) simulated ECC from the HFSS. [Color figure can be viewed in the online issue, which is available at wileyonlinelibrary.com]

environment are considered. The ergodic channel capacities are obtained by averaging over 10,000 Rayleigh fading realizations with a SNR ratio of 20 dB at the 10-antenna array. From the calculated results, the capacities in the 3.6-GHz band are about 43–47 bps/Hz. The maximum capacity is larger than four times that (about 11.5 bps/Hz [1]) of an ideal 2×2 MIMO system

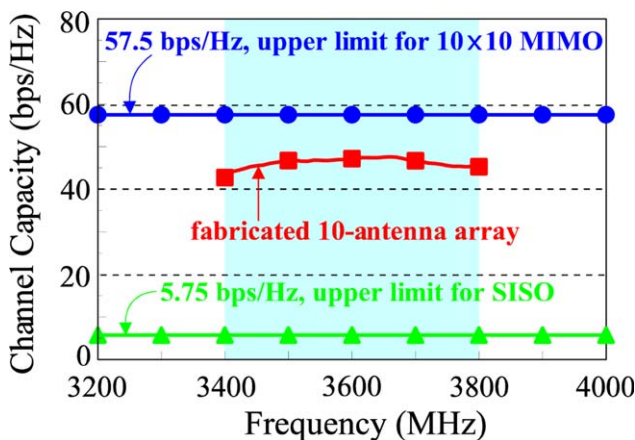


Figure 11 Calculated ergodic channel capacities of the fabricated 10-antenna array in a 10×10 MIMO system. [Color figure can be viewed in the online issue, which is available at wileyonlinelibrary.com]

(100% antenna efficiency and zero ECC between antennas) or about three times that (about 15.5 bps/Hz) of a 2×8 MIMO system [5].

4. CONCLUSION

A 3.6-GHz 10-antenna array in the smartphone has been proposed for the application in a 10×10 MIMO system. The 10-antenna array is disposed along the two long side edges of the system ground plane of the smartphone. Each antenna can cover the desired 3.6-GHz band (3.4–3.8 GHz) with acceptable antenna efficiency. Acceptable isolation of better than about 10 dB between antennas in the proposed array has also been obtained. Any two antennas in the proposed array also show good ECC of less than 0.1. Agreement between the measured data and simulated results of the proposed 10-antenna array has been observed. The calculated ergodic capacities of the 10-antenna array in a 10×10 MIMO system have been calculated to be about 47 bps/Hz with a 20-dB SNR, which is larger than about four times that (about 11.5 bps/Hz [1]) of an ideal 2×2 MIMO system. The proposed 10-antenna array is promising for the smartphone application in a 10×10 MIMO system.

REFERENCES

1. H. Li, Z.T. Miers, and B.K. Lau, Design of orthogonal MIMO handset antennas based on characteristic mode manipulation at frequency bands below 1 GHz, *IEEE Trans Antennas Propag* 62 (2014), 2756–2766.
2. M.S. Sharawi, Printed multi-band MIMO antenna systems and their performance metrics, *IEEE Antennas Propag Mag* 55 (2013), 218–232.
3. J. Guo, J. Fan, L. Sun, and B. Sun, A four-antenna system with high isolation for mobile phones, *IEEE Antennas Wireless Propag Lett* 12 (2013), 979–982.
4. S. Zhang, K. Zhao, Z. Ying, and S. He, Adaptive quad-element multi-wideband antenna array for user-effective LTE MIMO mobile terminals, *IEEE Trans Antennas Propag* 61 (2013), 4275–4283.
5. A.A. Al-Hadi, J. Ilvonen, R. Valkonen, and V. Viikari, Eight-element antenna array for diversity and MIMO mobile terminal in LTE 3500 MHz band, *Microwave Opt Technol Lett* 56 (2014), 1323–1327.
6. K.L. Wong, T.W. Kang, and M.F. Tu, Internal mobile phone antenna array for LTE/WWAN and LTE MIMO operations, *Microwave Opt Technol Lett* 53 (2011), 1569–1573.
7. K.L. Wong and M.T. Chen, Very-low-profile dual-wideband loop antenna for LTE tablet computer, *Microwave Opt Technol Lett* 57 (2015), 141–146.
8. C.I. Lin and K.L. Wong, Printed monopole slot antenna for internal multiband mobile phone antenna, *IEEE Trans Antennas Propag* 55 (2007), 3690–3697.
9. K.L. Wong and L.C. Lee, Multiband printed monopole slot antenna for WWAN operation in the laptop computer, *IEEE Trans Antennas Propag* 57 (2009), 324–330.
10. K.L. Wong, P.W. Lin, and C.H. Chang, Simple printed monopole slot antenna for penta-band WWAN operation in the mobile handset, *Microwave Opt Technol Lett* 53 (2011), 1399–1404.
11. ANSYS HFSS, Ansoft Corp., Pittsburgh, PA. Available at: <http://www.ansys.com/products/hf/hfss/>.
12. K.L. Wong and P.W. Lin, Compact dual-antenna with pi-shaped grounded strip for enhanced bandwidth and decreased coupling for LTE tablet computer application, *Microwave Opt Technol Lett* 57 (2015), 104–111.